Journal of Physics: Conference Series **3162** (2025) 012008 doi:10.1088/1742-6596/3162/1/012008

The XENONnT experiment: Latest results

Johan Loizeau
SUBATECH, IMT Atlantique, CNRS/IN2P3, Université de Nantes, Nantes 44307, France
E-mail: johan.loizeau@subatech.in2p3.fr

Abstract. The main goal of the XENONnT experiment is to prove the existence of WIMPs by directly detecting their interaction with a 5.9 t xenon target in a dual-phase Time Projection Chamber. In addition, thanks to the low background reached by the experiment, it is also possible to search for other rare events. A first science run corresponding to an exposure of 1.16 t·year of data was carried on in 2021: those data have been and are currently used to perform several analyses. The first was to verify an excess in electronic recoils observed in XENON1T experiment at low energy (below 30 keV). The electronic recoil background has been reduced by a factor of 5 compared to the previous experiment, reaching (15.8 ± 1.3) events/(t·y·keV), showing no hint of an excess on top of the expected backgrounds. Moreover, the WIMP search through the analysis of nuclear recoil events shows no significant excess. This leads to a minimum upper limit on the cross-section for the spin-independent WIMP-nucleon interaction of 2.58 × 10^{-47} cm^2 at a 28 GeV/c^2 WIMP mass with a 90% confidence level.

1. Introduction

Various astrophysical and cosmological observations indicate that dark matter comprises a significant fraction of the universe [1]. Among the numerous theories about dark matter composition, WIMPs (weakly interacting massive particles) are ones of the most promising candidates for a particle explanation of dark matter [2]. Those particles are expected to interact weakly with ordinary matter, so an experiment sensitive to rare events with a very low background is needed to detect the tiny signal issued by the collision of the dark matter particle with the target. Dual-phase time projection chambers (TPC) using liquid and gaseous xenon are among the best types of detectors for WIMP direct detection [3]. Indeed, with its high stopping power for gamma and beta radiation and its absence of long-lived isotopes, liquid xenon provides an excellent self-shielding with low internal radiation, making it an ideal medium for rare events searches. Moreover, with its large atomic mass (A ≈ 131), the expected rate of coherent elastic scattering between WIMPs and xenon nuclei is enhanced either in spin-dependent or spin-independent searches. The WIMP-nucleon collision is expected to induce a recoil with an energy of around 1 to 100 keV for a WIMP around a 100 GeV/c^2 mass. As only a few WIMPs events per year are expected to occur in a ton-scale liquid xenon (LXe) TPC detector [4], it's mandatory to reduce background as much as possible in order to be sensitive to such a rare process.

The XENON collaboration was founded in 2004 with the goal of proving the existence of WIMPs via the direct detection of their interaction with the liquid xenon target. Now including 27 institutions around the world, three detectors of increasing size, based on the TPC technology, had been operating: XENON10, XENON100 and XENON1T at the INFN Laboratori Nazionali del Gran Sasso (LNGS) below the Gran Sasso mountain in Italy. With 2 tonnes of liquid xenon

as a target, the XENON1T experiment was the first ton-scale dual-phase LXe TPC worldwide: it operated until the end of 2018. Now, the XENONnT experiment has a 3 times bigger target mass and a 5 times lower background in the WIMP search energy region than its predecessor. It is currently under data taking at LNGS [5] in order to shield it from cosmic background.

Moreover, the extremely low background opens the possibility to search for other interesting rare events physics channels. As an example electronic recoils can be used to search for neutrinoless double beta decay using ^{136}Xe naturally present in liquid xenon (with an abundance of 8.9%) [6], solar axion [7], ^{8}B coherent elastic neutrino-nucleus scattering CEνNS [8], or even supernova neutrinos.

In the next section, we will present the XENONnT experiment. Section 3 will be devoted to searches using electronic recoils at low energies. Finally, WIMPs results using nuclear recoils will be summarized in section 4.

2. The XENONnT experiment

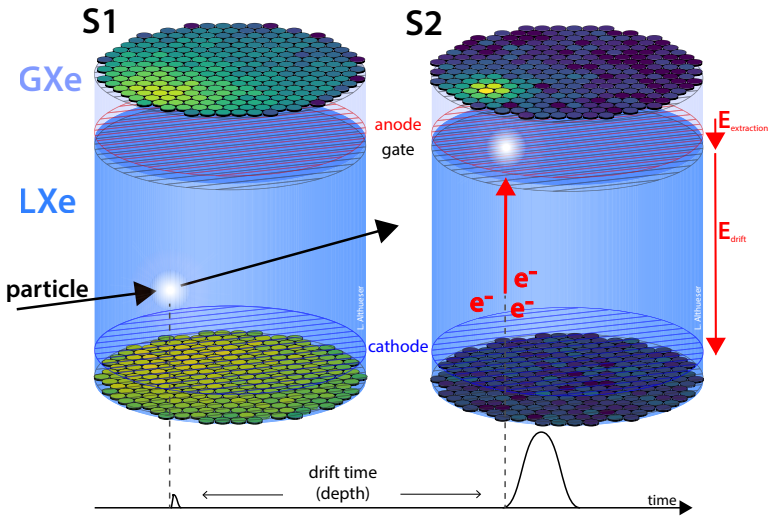

Figure 1: XENON experiment LXe dual phase detector working principle. (Left) An incident particle collides with a liquid xenon atom, emitting the first luminous signal S1. (Right) Free electrons are drifted by a first electric field and extracted to gaseous xenon phase by a second, stronger electric field and create the second luminous signal S2 [9].

The XENONnT experiment, the most recent experiment of the XENON collaboration, comprises several subsystems, some being reused from the previous XENON1T experiment, while others are newly developed. Both experiments use a dual-phase time projection chambers (working principle rendered in fig. 1) to detect incident particles. The XENONnT TPC measures ∼1.5 m in height and ∼1.3 m in diameter. In this TPC, the xenon detection volume is enclosed by 24 polytetrafluoroethylene (PTFE) reflector panels [4]. The active volume of 5.9 t of liquid xenon forms the target of incident particles. When such a particle interacts within the liquid xenon target, it will generate either a nuclear recoil (NR) if the particle is a WIMP or a neutron, or an electronic recoil (ER) if the particle is a photon, a charged particle or a neutrino [10]. In both scenarios, the collision with a xenon atom produces a first signal of light called S1 with a wavelength of 175 nm. This signal will be immediately detected by PMT arrays at the top and bottom of the detector of respectively 253 and 241 PMTs, chosen for their efficiency at 175 nm [13] and their low radioactivity [12]. Moreover, the collision emits free electrons.

Thanks to electric fields created by electrodes consisting of parallel wires placed around PTFE panels, those electrons will drift to the liquid-gas interface and then be extracted to the gas phase. Finally, electrons will interact with gaseous xenon, producing a second light signal called S2 detected by the same PMT arrays. The voltages applied to the electrodes are 4.9 kV for the anode, 700 V for the gate, and -2.75 kV for the cathode. Moreover, even if detected by the same PMTs, S1 and S2 signals have different shapes, allowing us to distinguish them. The events are then reconstructed by pairing S1 and S2 signals and used to determine the position of the interaction in the TPC. Indeed, the detection pattern on PMT arrays gives the (x,y) coordinates while the time difference between S1 and S2, corresponding to the drift-time of electrons, provides the depth of the interaction (z coordinate). For the following, signals will be referred to as cS1 and cS2, corresponding respectively to S1 and S2 signals corrected from all detector effects. Among those effects, we can list the non-uniformity of electric fields, quanta generation and collection efficiencies [11] or even electron lifetime correction. Those corrections are developed using calibration sources. This TPC is contained in a double-walled cryostat rendered in fig. 2 (left) and made of two stainless steel vessels, chosen in order to minimize material radioactivity in the WIMP energy domain.

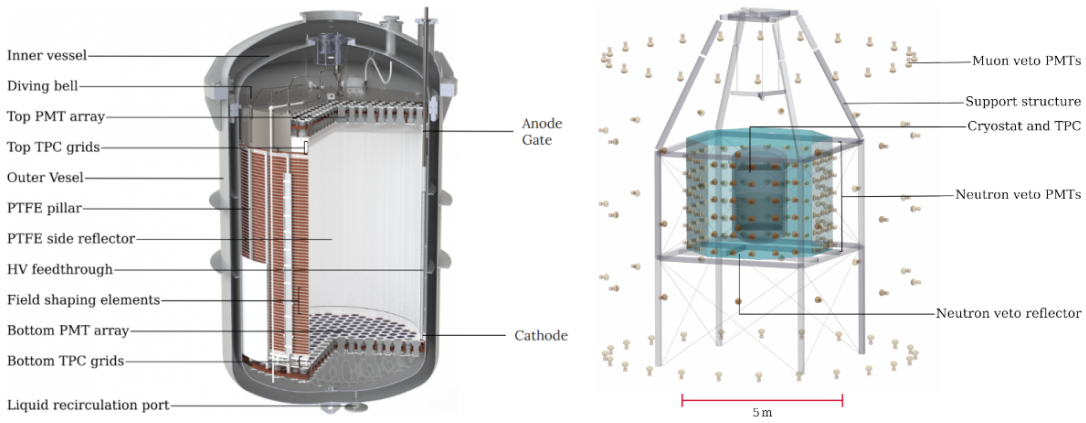

Figure 2: Left: Rendering of the XENONnT cryostat and TPC. The TPC has a diameter of ∼1.3 m and is ∼1.5 m-tall. Right: Rendering of the three nested detectors, including muon and neutron veto. The water tank walls are omitted for clarity. Reflector panels, which optically separate the neutron and muon vetos, are shown as transparent turquoise surfaces. The neutron veto PMT windows face the neutron veto region through openings in the panels [4].

The cryostat is placed in a ∼9.6 m-large and ∼10.2 m-tall stainless steel tank inherited from XENON1T. This tank filled with ∼700 t of water serves as a shield against environmental gamma and neutron radiations. Moreover, instrumenting the inner walls of the tank with PMTs allows operating as an active Cherenkov muon veto tagging muons from cosmic rays or cavern rock [14]. An additional neutron veto developed for XENONnT encloses the cryostat. It is made of PTFE reflective surfaces instrumented with additional 120 PMTs to detect the gamma-ray cascade after neutron capture in water [15] and thus further reducing background with a neutron tagging efficiency of 53 ± 3% [11]. The cryostat and both veto are rendered in fig. 2 (right).

To cool the liquid xenon inside the TPC to its operating temperature of $T_0 = -96^o$C, a cryogenic system is used [16]. Moreover, to reduce impurities and the concentrations of radioactive isotopes in xenon, various purification systems are used. Among them, a radon cryogenic distillation column [17] achieves an activity on 1.8 μBq/kg from ^{222}Rn for XENONnT first data acquisition and a krypton cryogenic distillation column to reduce the concentration of

krypton to 50 ppq ^{nat}Kr/Xe [18] allowing to have a low internal background. Additional liquid and gaseous xenon purification systems remove electronegatives impurities [19] treating 2 l of LXe per minute (350 kg per hour). Finally, two insulated stainless-steel storage named ReStoX (inherited from XENON1T) and ReStoX-II (built for XENONnT) are fundamental units to recuperate and store the xenon in case of emergency.

Moreover, numerous measures were taken during XENONnT construction to minimize the tritium in the form of tritiated hydrogen and tritiated water in the experiment. We can list the outgassing of the cryostat before its filling with GXe and all xenon purification campaigns performed [20].

Using the XENONnT experiment, a first science run called SR0 was performed between July and November 2021 corresponding to 97.1 days of data taking, allowing us to have a 1.16 t·year exposure to perform several blinded analyses.

3. Electronic recoil analysis

In 2020, the XENON1T experiment has observed an unexpected excess in electronic recoils (ER) events below ∼7 keV have been observed by the XENON1T experiment, as indicated by the blue dots in fig. 3 (left) [20]. Some interpretations beyond the standard model, such as solar axions, bosonic DM with a mass of ∼2.3 keV/c^2, and many other models [21] were proposed. However, this excess was also compatible with decays from trace amounts of tritium, which was not confirmed nor excluded.

Using the SR0 data collected by XENONnT, an ER analysis was performed to explore this energy region further. The ER background rate in (1, 30) keV was measured to be (15.8 ± 1.3) events/(t·y·keV) corresponding to a reduction factor ∼ 5 relative to the XENON1T rate. This value corresponds to the lowest ER background for the WIMP search in the field [5] and allows for a more precise and conclusive study that rejected at 4σ the excess observed by XENON1T as shown in fig. 3 (left). As the most likely explanation for this XENON1T excess is decays from tritium trace, the reduction campaigns of tritium in XENONnT presented in the previous section can explain its absence here.

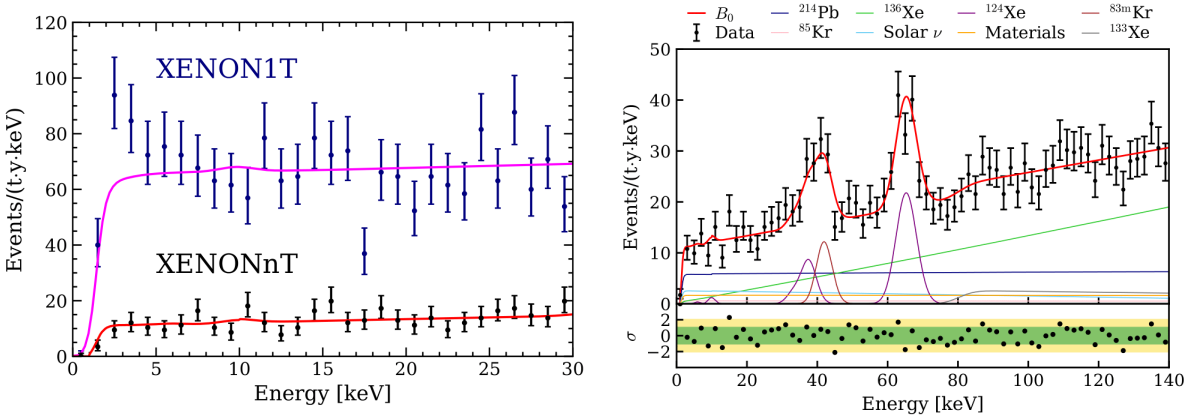

Figure 3: Left: ER data and best-fit model below 30 keV for XENON1T (blue dots and magenta line) and XENONnT (black dots and red line). No significant excess above the background was found in XENONnT [5, 20]. Right: Fit to SR0 data using the background model (B_0). The fit result of B_0 is the red line. A clear contribution is observed from second-order weak processes as $2\nu\beta\beta$ from ^{136}Xe and 2νECEC from ^{124}Xe [5].

Looking into the spectral shape of ER events within (1-140) keV displayed in fig. 3 (right), clear contributions of two second-order weak processes: $2\nu\beta\beta$ from ^{136}Xe and 2νECEC from

^{124}Xe are visible.

Moreover, using those data, new constraints were set on solar axions, bosonic DM, and solar neutrinos with an enhanced magnetic moment excluding new parameter spaces [5] as shown in fig. 4.

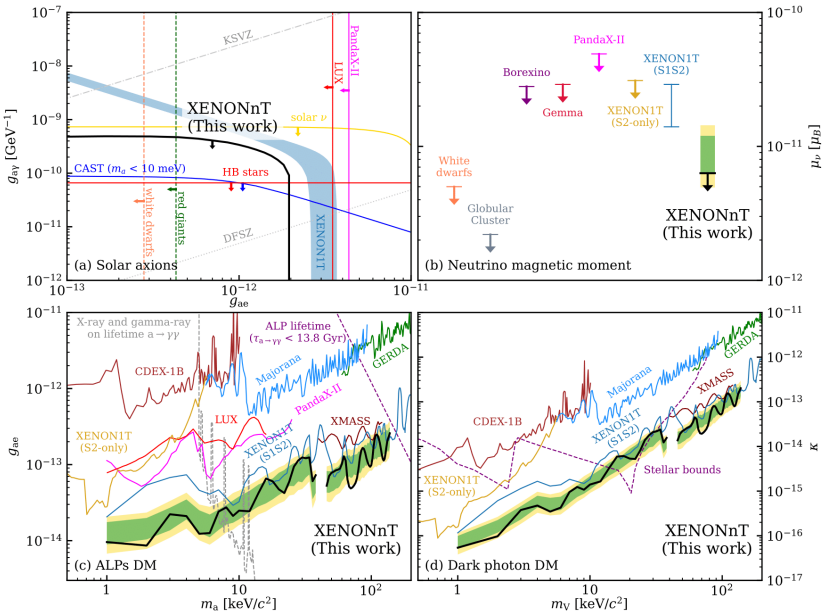

Figure 4: 90% C.L. upper limit on different new physics models. Constraints on the axion-electron g_{ae} and axion-photon $g_{a\gamma}$ couplings from a search for solar axions are shown in (a). Constraints on solar neutrinos with an enhanced magnetic moment (b), ALP DM (c), and dark photon DM (d) are shown together with the 1σ (green) and 2σ (yellow) sensitivity bands estimated with the background-only fit. Constraints between (39,42) keV/c^2 are excluded in (c) and (d) due to the unconstrained ^{83m}Kr background. Selected limits from other experiments and astrophysical observations are also shown [5].

4. Nuclear recoil analysis

As seen before, WIMPs are a potential candidate for dark matter composition. Those hypothetical particles should interact with xenon, inducing a nuclear recoil (NR). Using NR events from SR0, it is thus possible to put new constraints on the WIMP-nucleon cross-section. Among the NRs that occur in the TPC, the final efficiency depends on three major contributions. The first one is the detection efficiency of the detector, which is evaluated using a S1 3-fold simulation threshold and validated with a data-driven method [22]. The second one is from selection criteria optimized for this analysis [23]. Among them, data quality cuts are applied to suppress backgrounds by including only well-reconstructed events. Moreover, a dedicated cut was developed to reduce the background due to randomly paired S1-S2 signals called accidental coincidences (ACs). This cut uses data-driven models to look into the area and shape of S2, as well as the depth of the interaction, to reduce those ACs events [8]. The last contribution is the region of interest (ROI) defined to optimize WIMP detection [11].

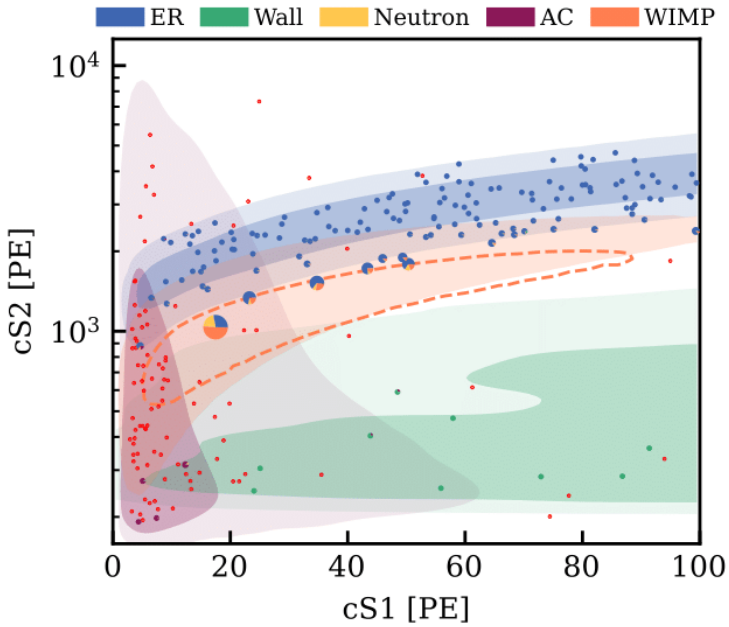

Figure 5: DM search data in the cS2-cS1 space. Each event is represented with a pie chart showing the fraction of the best-fit model, including the expected number of 200 GeV/c^2 WIMPs (orange) evaluated at the position of the event. The size of the pie charts is proportional to the signal model at that position. Background probability density distributions are shown as 1σ (dark) and 2σ (light) regions as indicated in the legend for ER (blue), AC (purple), and surface (green, "wall"). The neutron background (yellow in pies) has a similar distribution to the WIMP (orange-filled area showing the 2σ region). The orange dashed contour contains a signal-like region which is constructed to contain 50% of a 200 GeV/c^2 WIMP signal with the highest possible signal-to-noise ratio [11].

Table 1: Expected number of events for each model component and observed events. The "nominal" column shows expectation values and uncertainties, if applicable, before unblinding. The nominal ER value is the observed number of ER events before unblinding. The second column shows best-fit expectation values and uncertainties for a free fit, including a 200 GeV/c^2 WIMP signal component. The best-fit and nominal values agree within the uncertainties for all components [11].

	Nominal	Best fit
ER	134	135^{+12}_{-11}
Neutron	$1.1^{+0.6}_{-0.5}$	1.1 ± 0.4
CEνNS	0.23 ± 0.06	0.23 ± 0.06
AC	4.3 ± 0.2	$4.4^{+0.9}_{-0.8}$
Surface	14 ± 3	12 ± 2
Total background	154	152 ± 12
WIMP	–	2.6
Observed	–	152

In this ROI, the background model contains 4 major populations that are seen in fig. 5 showing the background probability density distributions of those populations in the cS2/cS1 parameter space:

- ER that was presented in the previous section. For the WIMP search, this background is dominated by β-decay from ^{214}Pb. This isotope comes from the ^{222}Rn chain.
- NR coming from two main sources: radiogenic neutrons not tagged by the neutron veto and neutrinos from CEνNS [8]. As WIMPs are supposed to interact as NR, it has a similar background probability density distributions.
- Surface background of ^{210}Pb contained in the TPC PTFE wall. Those surface events are mainly suppressed by a fiducial volume selection.
- Accidental coincidences previously defined are removed by a dedicated cut.

After unblinding the data, 152 events were found in the ROI, among which 16 were in the blinded WIMP region. Those data are shown in fig. 5 as pie charts, and their best-fit models are summarized in table 1. Thus, no significant excess was observed with the WIMP discovery p-value ($p \geq 0.20$). However, those data allow us to put new upper limits on the WIMP-nucleon interaction. The upper limit with a 90% confidence level on spin-independent interaction is displayed in fig. 6. Its lowest value of 2.58×10^{-47} cm^2 is reached at a 28 GeV/c^2 WIMP mass [11] corresponding to a factor ∼1.6 improvement from XENON1T results within a shorter period [24]. Furthermore, spin-dependent results show similar improvements (supplementary material from [11]).

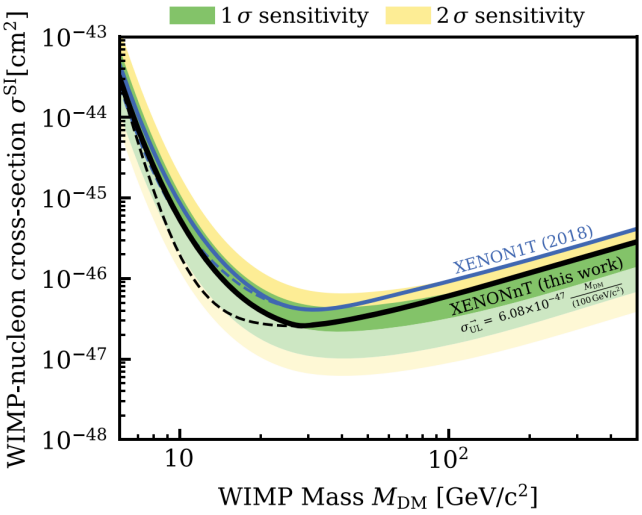

Figure 6: Upper limit on spin-independent WIMP-nucleon cross-section at 90% confidence level for XENONnT (full black line) as a function of the WIMP mass. A power constraint is applied to the limit to restrict it at or above the median unconstrained upper limit. The dashed lines show the upper limit without the power constraint. The 1σ (green) and 2σ (yellow) sensitivity bands are shown as shaded regions, with lighter colors indicating the range of possible fluctuations [11]. The result from XENON1T [24] is shown in blue with the same power constraint applied.

5. Summary and outlook

The XENONnT experiment performed a first science run of data taking with a 1.16 t·year exposure. Those data have been analyzed to perform several analyses where the lowest low-energy ER recoil background of (15.8 ± 1.3) events/(t·y·keV), 5 times better than XENON1T,

was achieved [5]. The analysis resulted in a rejection of the excess observed in XENON1T and in stronger constraints on new physics models. With NR data, a new spin-independent upper limit with a 90% confidence level was set reaching 2.58×10^{-47} cm^2 at a 28 GeV/c^2 WIMP mass. Furthermore, data collection with XENONnT is ongoing, and a further reduction of the ^{222}Rn activity to a level of 0.8 μBq/kg has been reached. Finally, an additional gadolinium doping of the neutron veto water was performed to enhance the neutron tagging efficiency and further reduce the NR background.

References

[1] G. Bertone, D. Hooper and J. Silk. Particle dark matter: evidence, candidates and constraints. *Physics Reports*, 405(5-6):279–390, Jan 2005.
[2] L. Roszkowski, E. M. Sessolo and S. Trojanowski. WIMP dark matter candidates and searches—current status and future prospects. *Reports on Progress in Physics, 81(6) :066201*, May 2018
[3] M. Schumann. Direct detection of WIMP dark matter : concepts and status. *Journal of Physics G : Nuclear and Particle Physics, 46(10) :103003*, Aug 2019.
[4] XENON collaboration. Projected WIMP sensitivity of the XENONnT dark matter experiment. *Journal of Cosmology and Astroparticle Physics, 2020(11):031-031*, Nov 2020.
[5] XENON collaboration. Search for new physics in electronic recoil data from XENONnT. *Physical Review Letters, 129(16)*, Oct 2022.
[6] XENON collaboration. Double-weak decays of ^{124}Xe and ^{136}Xe in the xenon1t and XENONnT experiments. *Physical Review C, 106(2)*, Aug 2022.
[7] Javier Redondo. Solar axion flux from the axion-electron coupling. *Journal of Cosmology and Astroparticle Physics, 2013(12):008–008*, Dec 2013
[8] XENON collaboration. Search for coherent elastic scattering of solar ^{8}B neutrinos in the xenon1t dark matter experiment. *Phys. Rev. Lett., 126:091301*, Mar 2021.
[9] L. Althüser. Search for Dark Matter and other beyond the Standard Model physics with XENON1T and XENONnT. PhD thesis, Münster (Westfalen). 2023.
[10] G. Plante. The XENON100 Dark Matter Experiment : Design, Construction, Calibration and 2010 Search Results with Improved Measurement of the Scintillation Response of Liquid Xenon to Low-Energy Nuclear Recoils. 2012
[11] XENON collaboration. First dark matter search with nuclear recoils from the XENONnT experiment. *Phys. Rev. Lett., 131:041003*, Jul 2023.
[12] XENON collaboration. Lowering the radioactivity of the photomultiplier tubes for the XENON1T dark matter experiment. *The European Physical Journal C, 75(11)*, Nov 2015.
[13] V.C. Antochi, L. Baudis, J. Bollig et al. Improved quality tests of r11410-21 photomultiplier tubes for the XENONnT experiment. *Journal of Instrumentation, 16(08):P08033*, Aug 2021.
[14] XENON collaboration. Conceptual design and simulation of a water Cherenkov muon veto for the XENON1T experiment. *Journal of Instrumentation, 9(11):P11006-P11006*, Nov 2014.
[15] Ll. Marti, M. Ikeda, Y. Kato et al. Evaluation of Gadolinium's Action on Water Cherenkov Detector Systems with EGADS, 2020.
[16] XENON collaboration. The XENON1T dark matter experiment. *The European Physical Journal C,77(12)*, Dec 2017.
[17] M. Murra, D. Schulte, C. Huhmann and C. Weinheimer. Design, construction and commissioning of a high-flow radon removal system for XENONnT. *The European Physical Journal C, 82(12)*, Dec 2022
[18] XENON collaboration. Removing krypton from xenon by cryogenic distillation to the ppq level. *The European Physical Journal C, 77(5):275*, 2017
[19] G. Plante, E. Aprile, J. Howlett and Y. Zhang. Liquid-phase purification for multi-tonne xenon detectors. *The European Physical Journal C, 82(10)*, Oct 2022
[20] XENON collaboration. Excess electronic recoil events in xenon1t. *Physical Review D, 102(7)*, Oct 2020.
[21] R. K. Leane, S. Shin, L. Yang et al. Snowmass2021 cosmic frontier white paper: Puzzling excesses in dark matter searches and how to resolve them, 2022.
[22] XENON collaboration. Xenon1t dark matter data analysis: Signal and background models and statistical inference. *Physical Review D, 99(11)*, Jun 2019.
[23] XENON collaboration. XENON1T dark matter data analysis: Signal reconstruction, calibration, and event selection. *Physical Review D, 100(5)*, Sep 2019.
[24] XENON collaboration. Dark Matter Search Results from a One Ton-Year Exposure of XENON1T. *Phys. Rev. Lett., 121(11)*, Sep 2018